

AEROACOUSTIC WIND TUNNEL TESTING AND CFD STUDY USING JAXA 8% SEMISPAN HIGH-LIFT COMMON RESEARCH MODEL IN JAXA FQUROH-2 PROJECT

Mitsuhiro MURAYAMA[1], Yo MURATA[1], Masataka KOHZAI[1], Kazuomi YAMAMOTO[1], Yasushi ITO[1], Hiroki URA[1], & Takehisa TAKAISHI[1]

[1]Japan Aerospace Exploration Agency, Aviation Technology Directorate, Mitaka, Tokyo, 181-0015, Japan

Abstract

This paper provides an overview of JAXA's aeroacoustic research in the FQUROH-2 project, which aims to demonstrate the effectiveness of low-noise concepts applied to a generic aircraft model, the CRM-HL, and to validate CFD-based prediction methods. As part of the project, a series of aeroacoustic wind tunnel tests have been conducted using a newly manufactured 8%-scale semispan CRM-HL. Various configurations, both with and without low-noise concepts, have been evaluated through the wind tunnel tests. Comparative studies between CFD and wind tunnel test results have been conducted to accurately predict noise from high-lift devices on practical aircraft configurations and to assess the capability of the noise prediction methods. This paper presents selected representative results based on the results obtained so far from these ongoing research activities.

Keywords: CRM-HL, High Lift Aerodynamics, Aeroacoustics, Wind Tunnel Test, CFD

1. Introduction

Airframe noise from high-lift devices and landing gear has become prominent as aircraft engine noise has been reduced, particularly during the approach conditions for landing when the engines are throttled down. The Japan Aerospace Exploration Agency (JAXA) has been making efforts to study airframe noise and its reduction techniques combining the numerical simulations with wind tunnel tests, focusing on high-lift devices (leading-edge slats and trailing-edge flaps) and landing gear [1-8]. In the Flight Demonstration of Quiet Technology to Reduce Noise from High-Lift Configurations (FQUROH) project, flight demonstrations have been successfully conducted to evaluate the effectiveness of noise reduction devices for the two-wheel main landing gear and flaps of JAXA's experimental research aircraft, "Hisho," which is based on the business jet Cessna Model 680 (Citation Sovereign) [1-2]. In this effort, JAXA collaborated with its domestic partner companies—Kawasaki Heavy Industries, Ltd ("KHI"), Mitsubishi Aircraft Corporation ("MITAC"), and Sumitomo Precision Products Co., Ltd. ("SPP")—to develop the concepts, conduct flight demonstrations, and mature the technologies. Through the series of flight tests and the validation studies by follow-on acoustic wind tunnel tests besides corresponding CFD analyses [3-4], the technology levels of design methodologies of noise reduction including the technologies of measurements and data processing have been significantly improved.

Subsequently, the FQUROH-2 project [9] started in 2024 to further mature the low-noise design methods and promote their application to medium-sized commercial aircraft. In this project, JAXA collaborates not only with the above-mentioned domestic partner companies but also with The Boeing Company and Safran Landing Systems to research and develop the low-noise technologies. As part of the FQUROH-2 project, a series of wind tunnel tests using scale models, together with CFD studies, has been conducted to demonstrate the effectiveness of the low-noise concepts applied to a generic aircraft geometry. For this purpose, a newly manufactured 8%-scale semispan

wind tunnel model based on the widely-used standard aircraft geometry, the High-Lift Common Research Model (CRM-HL), was introduced.

The CRM-HL is a standard model for takeoff and landing configurations with high-lift devices designed to represent modern commercial aircraft configurations under the leadership of NASA and Boeing [10-11]. The “CRM-HL Ecosystem” has been established, comprising research institutions and aircraft manufacturers around the world. One of the primary purposes of the CRM-HL Ecosystem is to verify the development of CFD technology for the aerodynamic analysis, design, and certification of high-lift configurations. Among them, several participants have already developed CRM-HL wind tunnel test models and conducted the wind tunnel tests [12-18]. JAXA has participated in the ecosystem as a member since 2020 and plans to contribute by sharing a subset of data from the wind tunnel tests.

In the FQUROH-2 project, four wind tunnel tests using the 8% semispan CRM-HL are planned. Tests #1 through #3 are scheduled in 2025 and 2026 at JAXA’s 6.5m × 5.5m Low-speed Wind Tunnel (herein referred to as “LWT1”), while Test #4 is planned in 2026 at Kawasaki’s 3m × 3m Low-speed aero-acoustic Wind Tunnel [12] (herein referred to as “KLWT”). During the series of wind tunnel tests, several configurations with and without low-noise concepts are evaluated [19-21]. Additionally, detailed acoustic wind tunnel tests on the CRM-HL main landing gear model alone have been performed [22-24]; however, these are beyond the scope of the present paper.

Comparison studies between CFD and wind tunnel test results have been conducted to accurately predict noise from high-lift devices on practical aircraft configurations and to assess the capability of the noise prediction methods [25-27]. This paper provides an overview of these research activities, focusing on the effectiveness of the low-noise concepts applied to the CRM-HL slats and on the validation of CFD-based prediction methods. Selected representative results are presented based on acoustic measurements obtained during the first test conducted between April and May 2025 at LWT1 (LWT1 Test #1) and the corresponding CFD results. Our companion paper [28] presents the wind tunnel test results on the detailed aerodynamic characteristics of the 8% semispan CRM-HL at LWT1 (LWT1 Test #2).

2. Experimental Set-ups

2.1 Test Schedule

Table 1 shows the current schedule for the series of wind tunnel tests planned at JAXA. Two major research topics on the airframe noise reduction (FQUROH-2 project) and the stall prediction are ongoing in conjunction with these wind tunnel tests. In total, six wind tunnel tests using the 8% semispan CRM-HL are planned. In the FQUROH-2 project, four wind tunnel tests are included. Tests #1 through #3 have been completed in 2025 and 2026 at LWT1, while Test #4 is planned for the summer of 2026 at KLWT. Tests #1 and #3 were primarily for airframe noise research, including noise source identification using a microphone array, as well as measurements of aerodynamic forces and moments and steady and unsteady surface pressures. Test #2 was primarily for stall prediction research, including detailed aerodynamic measurements together with flowfield investigation using particle image velocimetry (PIV) and oil-flow visualization. In addition, the effects of noise-reduction devices on the wake flow behind the main landing gear are investigated using PIV. Following these four tests, two tests are planned at LWT1. Test #5, scheduled for 2026, will focus on model deformation measurement (MDM) and total pressure distribution of the floor boundary layer using Pitot-lake measurements. Test #6, scheduled for 2027, will focus on pressure sensitive paint (PSP) measurements.

This paper provides selected representative results obtained at the first Test #1, conducted between April and May 2025 at LWT1.

Table 1 - Current schedule for the series of CRM-HL wind tunnel tests planned at JAXA.

	2024	2025	2026	2027	2028
Airframe noise reduction research (FQUROH-2)		Model delivery; LWT1 Test #1 Noise data; LWT1 Test #2 PIV data	LWT1 Test #3 Noise data; KLWT Test #4 Noise data		
Stall prediction research		LWT1 Test #1 Validation data; LWT1 Test #2 Detailed aero. data, 3D-PIV and Oil flow	LWT1 Test #5 MDM and Pitot-lake	LWT1 Test #6 PSP	

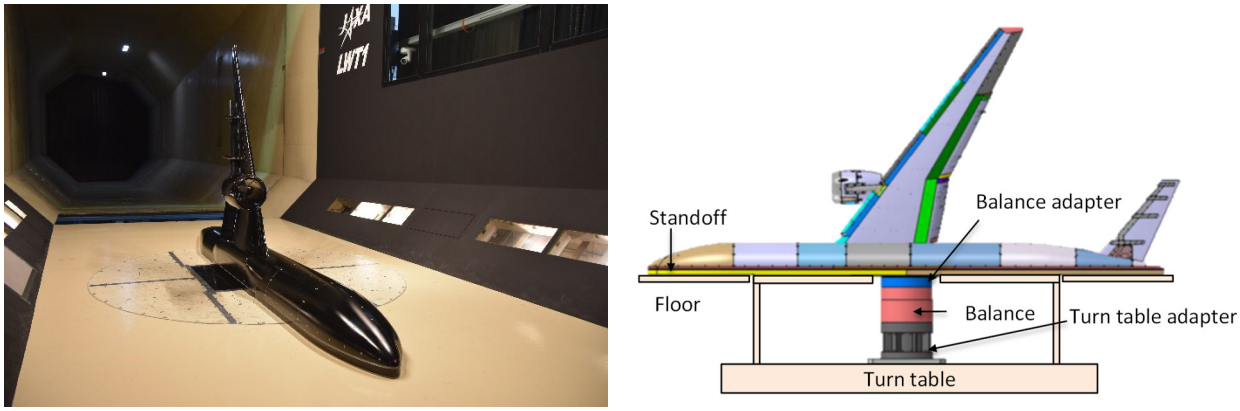
2.2 Test Facility and Model Geometry

LWT1 is a closed-circuit, continuous-atmospheric wind tunnel. The test section has an octagonal cross-section, measuring 6.5 m in height and 5.5 m in width, with 1 m truncations at each corner, and has a length of 9.25 m. The contraction ratio is 1:5.33, and the maximum wind speed is 70 m/s. ~~In the test setup, a turntable was installed on a strut cart without any model support, and the angle of attack (AoA) was varied by controlling the turntable.~~

The test utilized JAXA's newly manufactured 8%-scale semispan CRM-HL (hereafter referred to as "JAXA 8% SS CRM-HL"). This model is based on the geometry defined and presented in the CRM-HL Ecosystem and is designed for testing in both JAXA's LWT1 and KHI's KLWT. The model configuration can be identical to the so-called "NASA 5.2% semispan model" of the CRM-HL geometry [15]. In this study, the configuration, which has a flow-through nacelle with a chine, but does not include horizontal or vertical stabilizers, was used. The nominal inboard and outboard flap deflections at 40 degrees and 37 degrees, respectively, were used.

In addition to the CRM-HL Ecosystem landing configuration, the JAXA 8% SS CRM-HL can reproduce the 8%-scale version of the NASA 10% semispan acoustic baseline CRM-HL geometry (hereafter referred to as "NASA-rep" configuration), which was used in earlier acoustic wind tunnel tests at the NASA Langley 14-by-22-foot low-speed wind tunnel. This configuration differs from the CRM-HL Ecosystem configuration in the settings of the slats and flaps, as well as in the designs of the slat tracks and flap track fairings (FTFs). The detailed comparison of the aeroacoustic characteristics between the CRM-HL Ecosystem landing configuration and the "NASA-rep" configuration is provided in Ref. 21

Figure 1 shows the JAXA 8% SS CRM-HL installed in the LWT1 test section. The fuselage mounting base is fixed to the tunnel turntable with a turntable adapter, a five-component balance, and a balance adapter. To reduce the influence of the boundary layer on the wind tunnel floor, a standoff is introduced to elevate the fuselage symmetry plane above the floor. Based on prior measurements of the floor boundary layer, which showed a displacement thickness of 15 mm at wind speeds between 50 m/s and 70 m/s, the standoff with a height of 60 mm was used in the tests. The inboard slat consists of a single piece, while the outboard slat comprises three pieces of approximately equal span length, designated from the outermost as #1, #2, and #3. The flaps consist of two pieces, one on the inboard side and the other on the outboard side. Further details of LWT1 and the model geometry are provided in Refs. [20, 28].



(a) Model installed in the test section. (b) Schematic of model installation.

Figure 1 - JAXA 8% SS CRM-HL model mounted in JAXA's 6.5m × 5.5m low-speed wind tunnel.

2.3 Test Conditions

The Mach number was set to 0.2 as the reference wind speed as defined in the CRM-HL Ecosystem. During the Mach 0.2 tests, the airflow temperature varied from approximately 20°C to 22°C, resulting in wind speeds ranging from 70 m/s to 71 m/s. The Reynolds number, based on the mean aerodynamic chord (MAC) of 0.5604 m, ranged from 2.4×10^6 to 2.5×10^6, influenced by the change in the airflow temperature. Measurements were performed varying the AoAs from 0 degree to a maximum of 21 degrees. The acoustic measurements were conducted up to 12 degrees. In this test, in addition to the 8-degree angle tested at NASA with their 10% semispan model, 4 degrees was also defined as a reference AoA, which was considered more suitable for evaluating noise during the landing approach.

2.4 Measurements

Five-component force and moment measurements, surface static pressure measurements, surface unsteady pressure measurements, tuft measurements, and noise source identification using a phased array system were performed in the first test. The number of points for each measurement is shown in Table 2. Details of the aeroacoustic and aerodynamic measurement methods are provided in Refs. [20-21, 26].

Table 2 - Types and number of measurement points.

Measurement type	Number of measurement points
Five-component force and moment	-
Acoustic array (Noise source identification)	1 (with 96 microphones)
Surface static pressure	433
Surface unsteady pressure	16
Tuft visualization	-

Acoustic measurements were conducted using a phased array system mounted on the starboard-side corner wall, as shown in Fig. 2, together with an example of beamforming results. The array consisted of 96 microphones arranged in an elliptic layout with a characteristic dimension of 1m and was positioned approximately 90 degrees relative to the model's lower surface. A windscreen was installed over the array, with the windscreen surface flush-mounted to the wind tunnel wall.

Conventional beamforming analysis was performed on the measured acoustic signals, identifying the noise sources on the model. The diagonal part in the cross-spectral matrix was removed in the conventional beamforming analysis. The analysis plane was designed to follow the main wing, considering the dihedral angle. The noise-source localization maps presented in this paper were generated for each 1/3-octave-band center frequency and are shown at the 8% model scale without further scale conversion. Two corrections were applied to the narrowband pressure data prior to noise-

map generation: normalization to a 1-m reference source distance and atmospheric-absorption correction using ISO 9613-1 to account for propagation differences between facilities. After the noise-source localization maps were generated, sound-pressure signals were integrated over specified analysis regions to obtain the corresponding spectra.

When the overall sound pressure level (OA) is evaluated, a scale conversion was applied to the spectrum, converting the measured model scale spectrum to an equivalent full-scale spectrum. This conversion considered the model scale, measurement distance, and wind speed. The model scale, measurement distance, and wind speed were set to 8%, 120 m, and 68.21 m/s, respectively. Frequency scaling was also applied, assuming a constant Strouhal number and using the representative length and uniform flow velocity. For comparison with CFD results at the measured model scale, only the measurement distance was adjusted from 1m to 120m.



Figure 2 – Phased array system mounted on the LWT1 wall and example of beamforming results.

3. Numerical Methods

3.1 Computational Methods and Flow Solvers

In recent years, two notable techniques incorporated into CFD solvers for computational aeroacoustics (CAA) are the turbulent wall model and the Lattice-Boltzmann method. Wall models integrated into Large-Eddy Simulations (WM-LES) or LBM-based Very Large Eddy Simulations (LBM-VLES) can significantly reduce computational costs while effectively resolving highly unsteady flows, including turbulent boundary layers. These approaches, WM-LES and LBM-VLES, combined with sound projection techniques using the Ffowcs-Williams & Hawkings (FW-H) method have become widely-used CAA approaches for predicting airframe noise. Several WM-LES approaches have been evaluated, including comparison with CRM-HL wind-tunnel test data in Refs. [25, 27]. JAXA has mainly focused on evaluating LBM-VLES [25-26], with the aim of developing efficient grid strategies, turbulence treatments, and FW-H strategies for accurate noise prediction from high-lift devices on practical aircraft configurations. This paper presents results obtained using the LBM-VLES.

The LBM-VLES simulations were performed using a commercial CFD code, PowerFLOW, which solves compressible flows based on the three-dimensional 19-state (D3Q19) LBM. The method has been extended to solve higher Mach number flows. This solver models the near-wall region of the turbulent boundary layer using an algebraic wall model including a pressure gradient. The combination of the LBM-VLES and the wall model exhibits conceptual similarities to the hybrid RANS/LES approach. The solver provides efficient predictions of turbulent flows in practical engineering applications at high Reynolds numbers. All airframe surfaces were treated as fully turbulent boundary layers in this study.

3.2 Computational Conditions

Figure 3 shows an example of the computational grids used in this study. PowerFLOW solves the flow in a hierarchical cubic Cartesian mesh with an immersed boundary condition. In addition to the

surface grids, we resolve some volumetric spaces to preserve high-frequency acoustic waves until they reach the permeable FW-H surfaces. In the current study, these volumetrically refined regions are created along the outboard slat and near the outboard side edge of the outboard flap, as shown in Fig. 4. The computational grid consists of 14 variable resolution (VR) levels, with a minimum spacing of 0.287mm. The finest VR14 regions cover only the cusps and trailing edges of the slats and the flaps as well as the main wing. The leading-edge box is the second refined region, while the trailing-edge box is the third refined region. The total grid count is about 1.18 billion voxels. For the permeable FW-H surfaces, an end-cap averaging technique was used, as defined in Fig. 4. For the permeable FW-H around the flap side-edge, we prepare three types of end-cap configurations for end-cap-averaging: the first set has the baseline surfaces with eight end-caps, the second set also has eight caps, but the spacing is half of that for the baseline with the same downstream end, and the last set has only four end-caps located further downstream of the original FW-H surface end. In our previous study [26], the results were relatively insensitive to the number of the end-caps, their spacing, and their downstream locations in a reasonable extent. In this study, therefore, we will present results using the baseline surfaces with eight end-caps for the flap side-edge regions. Based on our previous experience, five end-caps are used for the outboard slat regions in the FW-H averaging process.

In this study, the freestream Mach number and angle of attack were set to M = 0.2 and AoA = 8 degrees. The Reynolds number, based on the mean aerodynamic chord, was set to be Re = 2.62 × 10^6, which is slightly higher than the experimental conditions due to the difference in temperature. However, the difference in the Reynolds number is small enough to discuss between the computational results and wind tunnel test results. Therefore, we kept *Re* = 2.62 × 10^6 in the simulations.

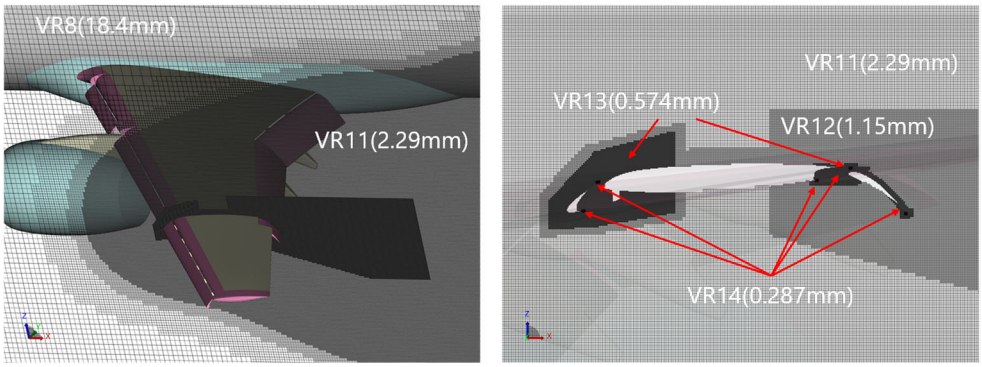
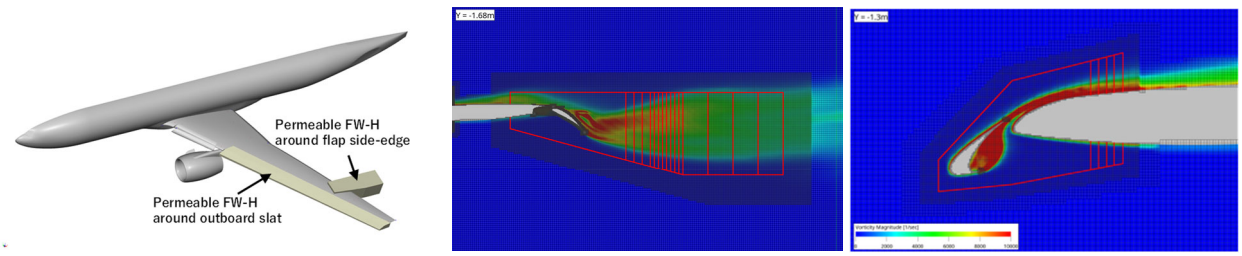


Figure 3 - Computational grid around the CRM-HL geometry cut at an outboard section.



(a)Flap side-edge at Y=1.68m. (b)Outboard slat at Y=1.3m.

Figure 4 - Permeable FW-H definition around the flap side-edge and outboard slat and cross-sectional views of the permeable FW-H definition around (a) the flap side-edge and (b) the outboard slat, along with the computational grid and time-averaged voriticity magnitude.

4. Noise Reduction Devices Applied to Slat

In this paper, the noise reduction devices applied to the slats are shown. The noise reduction devices are based on research conducted in the FQUROH-2 project and its predecessors [1-8]. Each device can be retrofittable, applicable to various aircraft geometries. To demonstrate the effectiveness of

these devices, evaluation using the CRM-HL, a publicly available common geometry, is considered highly meaningful.

Figure 5 shows a representative flowfield around a slat and slat noise reduction concept used in this study. The shear layer emanating from the slat cusp and its subsequent reattachment upstream of the slat trailing-edge (TE) lead to a primarily broadband noise spectrum. As a countermeasure, JAXA, KHI, and MITAC developed a low-noise concept as shown in Fig. 5 that combines a TE extension and a small cove bump [7-8]. This concept increases the distance between the flow reattachment point in the cove region and the slat TE. As a result, the distance over which pressure fluctuations attenuate before reaching the TE after reattachment increases. Moreover, the TE extension reduces the gap between the slat and the leading edge (LE) of the main wing. This reduces the flow velocity around the slat tracks, which correspond to the slat brackets in the wind tunnel model, as well as around the cutouts, both of which are other significant major noise sources. Figure 6 shows the slat noise-reduction devices implemented to the JAXA 8% SS CRM-HL.

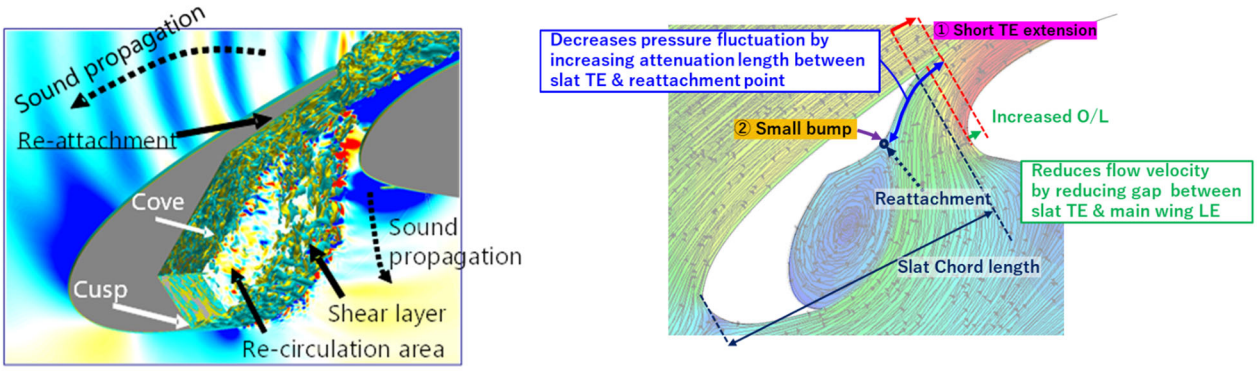
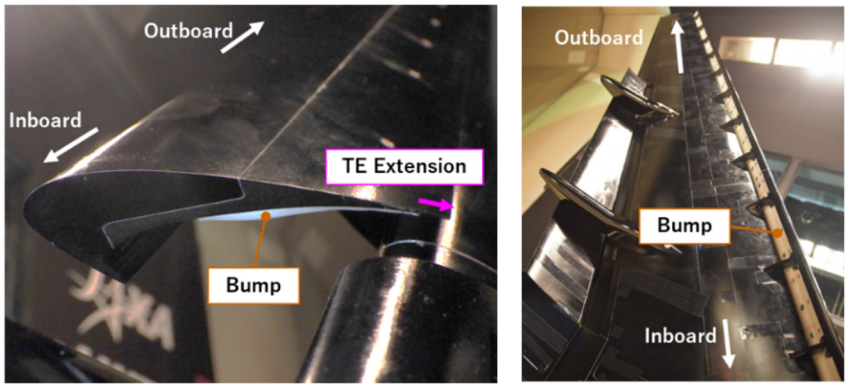


Figure 5 - Mechanism of slat noise reduction concept used in this study.



(a) Side view (b) Lower side

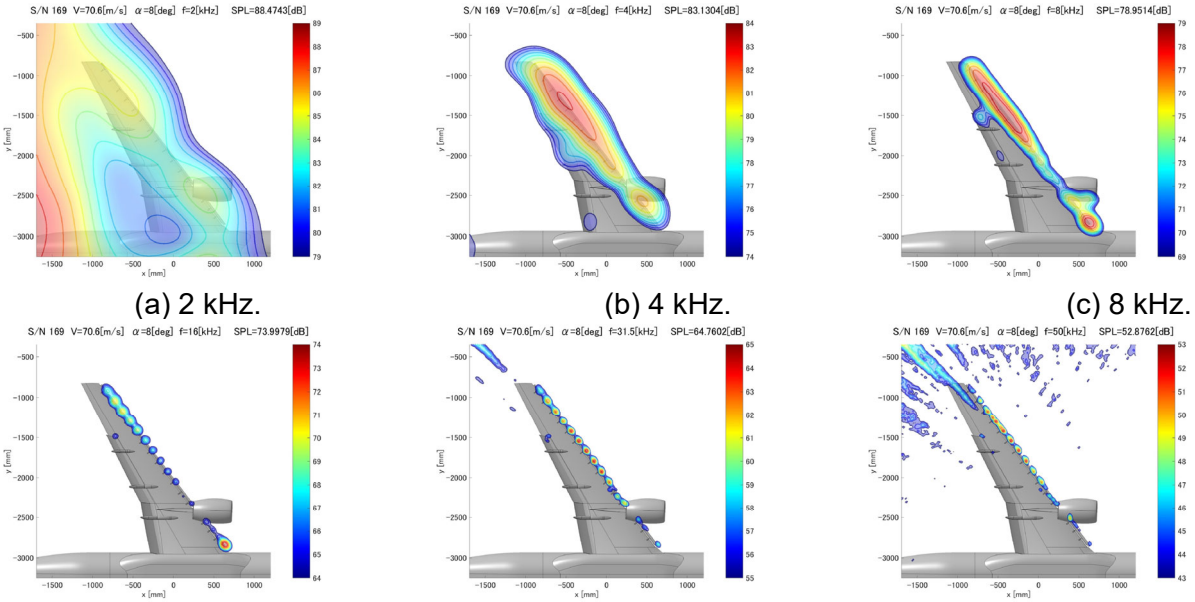
Figure 6 - Slat noise-reduction devices implemented to the JAXA 8% SS CRM-HL.

5. Results

Figure 7 shows noise source maps for the baseline configuration without noise reduction devices, processed with conventional beamforming at selected frequencies ranging from 2 kHz to 50 kHz in the model-scale, obtained in the JAXA LWT1. In this frequency range, signal-to-noise ratio and spatial resolution of the noise source maps are acceptable for our analysis. The noise sources around the slat are clearly captured. At higher frequencies, noise by the slat tracks becomes dominant. Under the current test conditions, the outboard flap side edge noise is relatively weak compared to the slat noise.

Figure 8 shows comparison of noise maps for the 1/3-octave band at 31.5 kHz (2.5 kHz in full scale) for the baseline configuration and the configuration with slat noise devices installed. For ease of comparison, the baseline result shown in Fig. 7(e) is reproduced in Fig. 8(a). The result with the slat

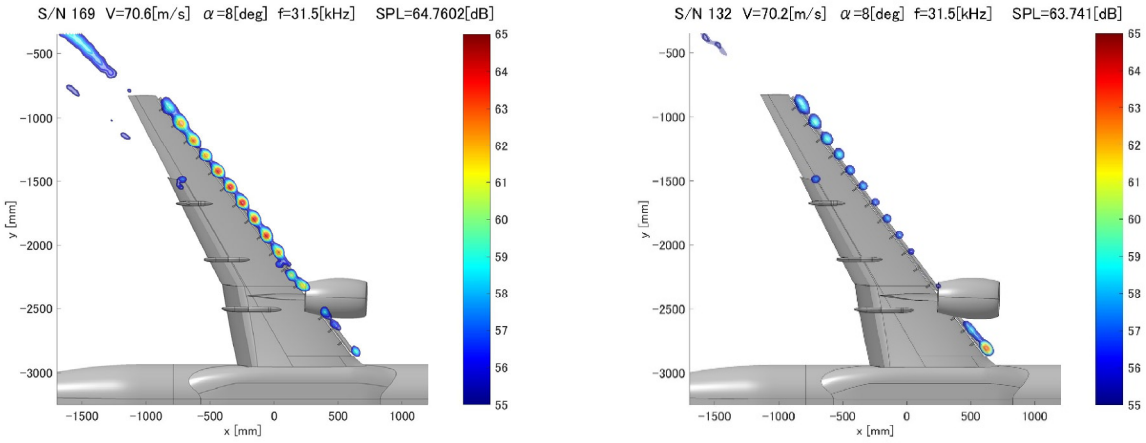
noise devices shown in Fig. 8(b) clearly shows reduction of SPLs for each source around the slat and brackets when compared to the baseline result shown in Fig. 8(a). Figure 9 compares the spectra obtained by integrating the outboard slat region for each configuration. The spectra were converted from 8% to full-scale. Compared to the result for the baseline configuration, the result with the slat devices reduced the noise across nearly all bands below 3 kHz. A significant overall noise reduction effect over 3 dBA was obtained with the slat noise devices installed. Although noise levels increase around 4 kHz with the devices installed, this is considered due to enhanced vortex shedding from the slat trailing edge with the devices. The tone generated by the vortex shedding from the slat trailing edge is particularly more noticeable under low Reynolds number conditions in the wind tunnel test. As the Reynolds number increases, the coherent vortex structures in the spanwise direction decrease, leading to a reduction in the peak sound pressure level. In addition, the slat trailing-edge thickness of the CRM-HL can be generally thicker than that of the actual aircraft. If the trailing-edge thickness becomes thinner, the frequency of the resulting tone shifts to a higher frequency range, which results in the reduction of the contribution to the overall sound pressure level at the full-scale.



(a) 2 kHz. (b) 4 kHz. (c) 8 kHz.

(d) 16 kHz. (e) 31.5 kHz. (f) 50 kHz.

Figure 7 - Noise source maps for the baseline configuration without noise reduction devices obtained in the JAXA LWT1.



(a) Baseline without slat devices (b) With slat devices

Figure 8 - Comparison of noise maps at 31.5 kHz (2.5 kHz at full scale) with and without slat devices. (Figure 8(a) is reproduced from Fig. 7(e) for ease of comparison.)

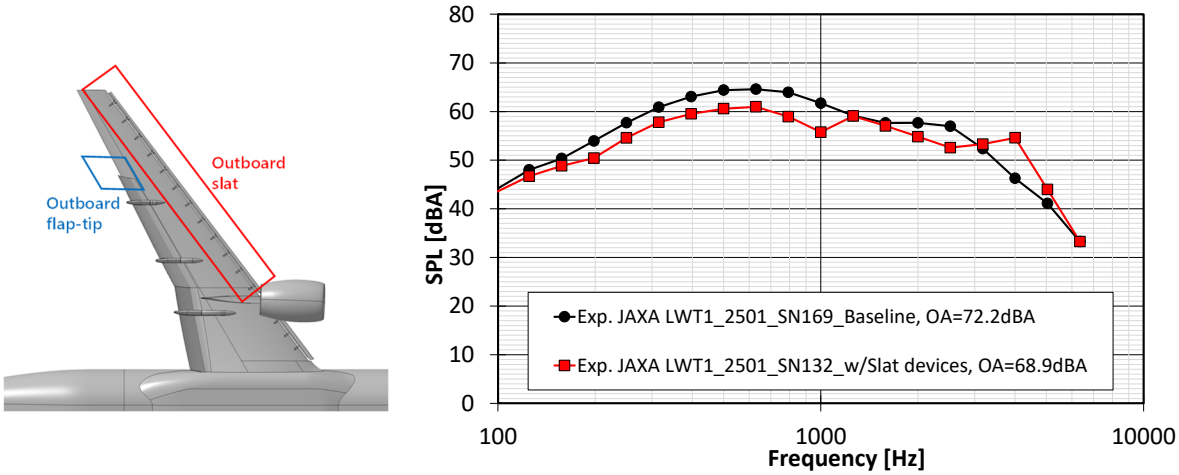
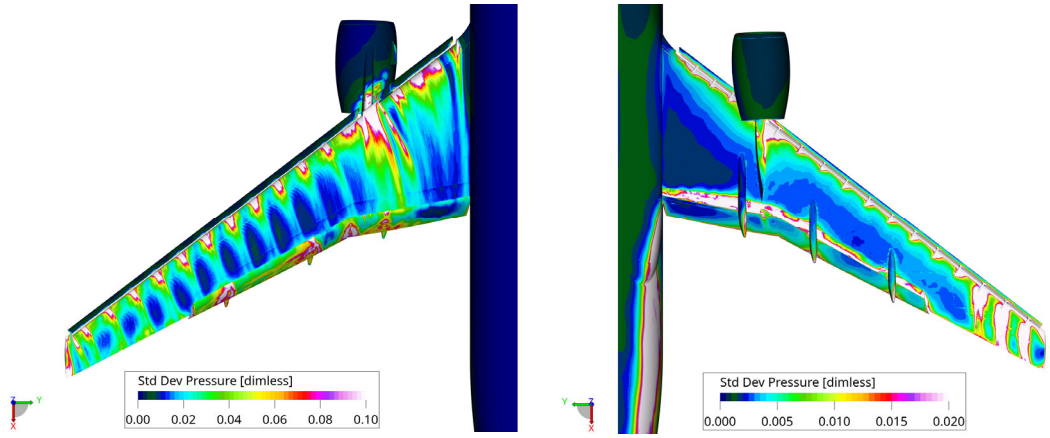


Figure 9 - Comparison of integrated 1/3 octave band spectra of the outboard slat domain with and without devices (converted to full scale).

Next, the computational results are compared with the wind tunnel test results to evaluate the performance of the CFD-based prediction methods. Figure 10 shows computational results of the wall pressure fluctuation (standard deviation of static pressure, denoted by P_{rms}) on the model surface for the baseline configuration. On the suction side, the computational result shows high P_{rms} along the wake generated by the slat tracks and the nacelle-pylon. High P_{rms} regions are also found at flow separations observed over the flap, particularly around the FTFs and the junction between the inboard and outboard flaps. On the pressure side, high P_{rms} regions are found around the slat and along the wake from three slat tracks on the outboard wing.

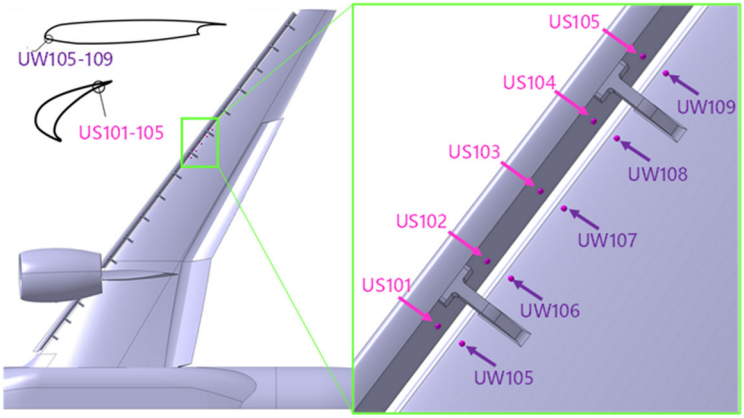
Figure 11(a) shows the locations of Kulite dynamic sensors to measure unsteady pressure on the model surface in the wind tunnel test at LWT1. The sensors labeled US101 to US105 are located on the pressure side of the outboard slat at 83% of the slat's local chord length and are aligned in a spanwise direction. Sensors labeled UW105 to UW109 are located on the pressure side of the outboard main wing at 2% of the main wing's chord length, with their spanwise locations corresponding to those of sensors US101 to US105. Figure 11 compares the computational and wind tunnel test results for Power Spectral Densities (PSDs) measured at several selected sensor locations. Data obtained under no-wind conditions are also included in the graph to show the influence of the sensors' electrical noise. Sensor US103 is located in the middle of the two slat brackets; therefore, the influence due to the slat brackets is minimal. Sensor US102 is located downstream on the outboard side of each slat to investigate the influence of slat tracks. The computational results at US103 and UW107, which are located in the middle of the two slat brackets where the influence of the slat brackets is minimal, show very good agreement with the Kulite spectra particularly in the frequency range below 20 kHz. With the grid resolution of VR13 = 0.574mm around the slat cove, the current simulation can resolve acoustic waves up to approximately 50 kHz, whereas the smallest-scale vortices have a frequency of about 20-24 kHz. Therefore, the computed spectra are underpredicted, particularly at high frequencies. On the other hand, the computational result at US102, which is located downstream on the outboard side of each slat track, slightly tends to overpredict the Kulite spectra below 20 kHz. The flow disturbed by the slat track makes the simulations difficult to accurately capture unsteady fluctuations.

Figure 12 compares the noise spectra of the outboard slat obtained from the computation and the wind tunnel test. The computational results were obtained using the permeable FW-H method around the outboard slat with the end-caps averaged, while the wind tunnel test results were obtained by integrating the noise source map around the outboard slat. The spectra were evaluated at the original 8% wind tunnel test scale. The computational result shows generally good agreement with the experimental data for frequencies below 50 kHz. These results validate the reasonable accuracy of current prediction methods for slat noise prediction in the baseline configuration.

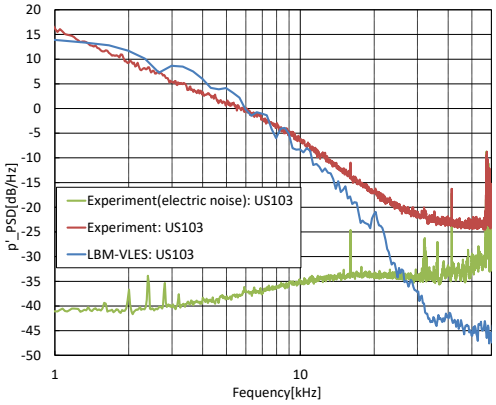


(a) Suction side. (b) Pressure side.

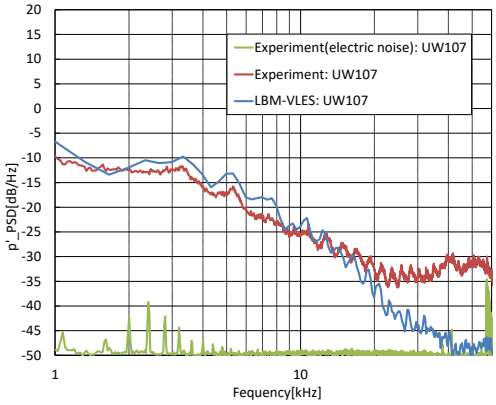
Figure 10 - Computational results of wall pressure fluctuation for the baseline configuration.



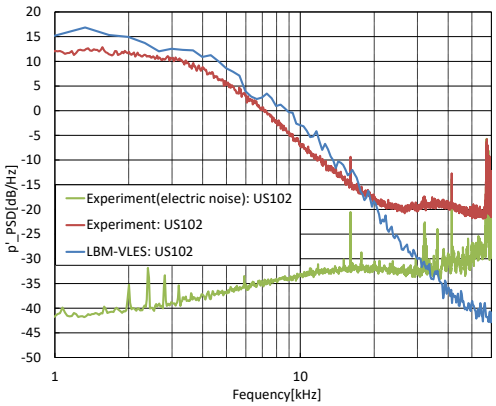
(a) Kulite locations in the wind tunnel test at JAXA LWT1.



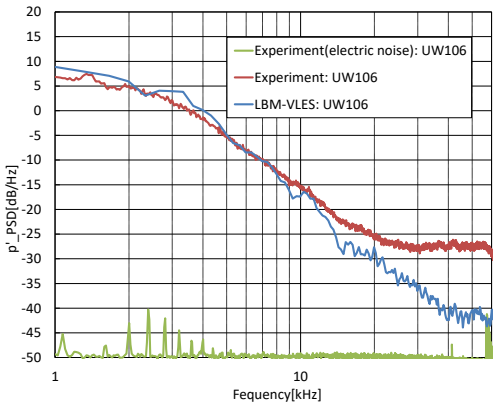
(b) US103.



(c) UW107.



(d) US102.



(e) UW106.

Figure 11 - Comparison of PSD with Kulite data measured at JAXA LWT1.

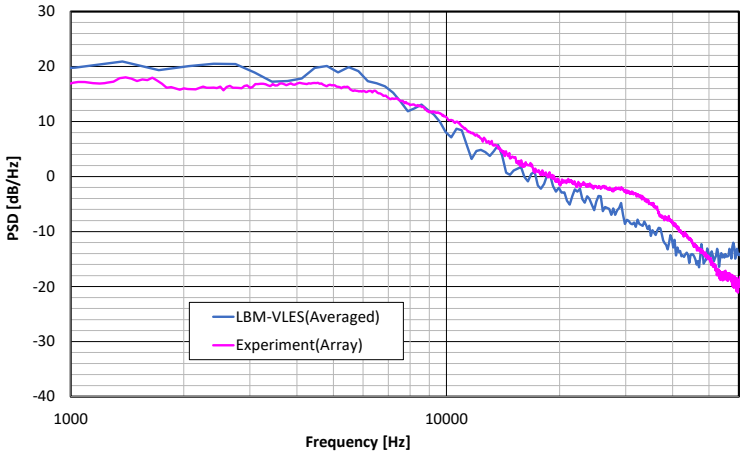
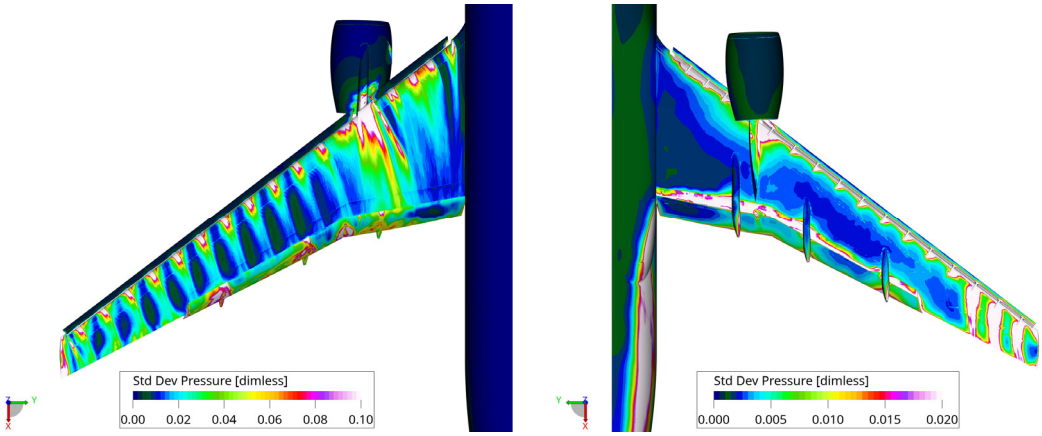


Figure 12 - Comparison of the outboard slat noise levels at a directivity angle of 98 degrees between the computational result obtained using permeable FW-H around the outboard slat with the end-caps averaged and the wind tunnel test results obtained by integrating the noise source map around the outboard slat.

Next, the computational results for the configuration with slat noise reduction devices are shown. Figure 13 shows computational results of the wall pressure fluctuation on the model surface. The results with the slat noise reduction devices clearly show a reduction in regions with high pressure fluctuations. Figure 14 compares the computed 1/3 octave band spectra of the outboard slat at a directivity angle of 98 degrees, with and without noise reduction devices. The spectra and frequency are converted to full scale. Figure 15 compares the corresponding ΔSPL by the slat noise reduction devices, relative to the baseline configuration around the outboard slat between computational and wind tunnel test results. Both computational and wind tunnel test results clearly show the effectiveness of the slat noise reduction devices. A slight difference is observed around the peak due to the trailing-edge, where a peak increase is observed in the wind tunnel test with the devices. This difference may derive from limitations in grid resolution around the trailing-edge. Nevertheless, the comparison studies between the computational and experimental results for the CRM-HL demonstrate the reasonable accuracy of current CFD-based prediction methods, not only for the baseline configuration but also for predicting ΔSPL by noise reduction devices for realistic high-lift configurations.

Figure 16 compares sectional views of computational results at Section 5, passing through the mid-span of the outboard slat, for the configurations with and without slat noise reduction devices. With the TE extension and the small cove bump, the Mach number contours and streamlines show that the shear layer emanating from the slat cusp reattaches near the top of the designed bump as intended. This reduces pressure fluctuations around the reattachment point and increases the distance between the flow reattachment point and the slat TE, leading to decay of pressure fluctuations before reaching the TE. Overall, computational results provide physical insights into the noise generation and reduction mechanisms associated with slat cove flows and their change by the slat noise reduction devices.



(a) Suction side. (b) Pressure side.

Figure 13 - Computational results of wall pressure fluctuation for the configuration with slat noise reduction devices installed.

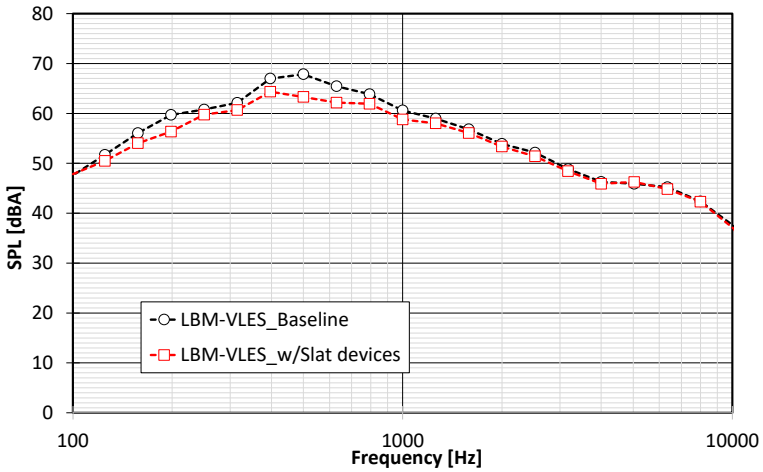


Figure 14 - Comparison of computed 1/3 octave band spectra of the outboard slat at a directivity angle of 98 degrees, with and without noise reduction devices (converted to full scale).

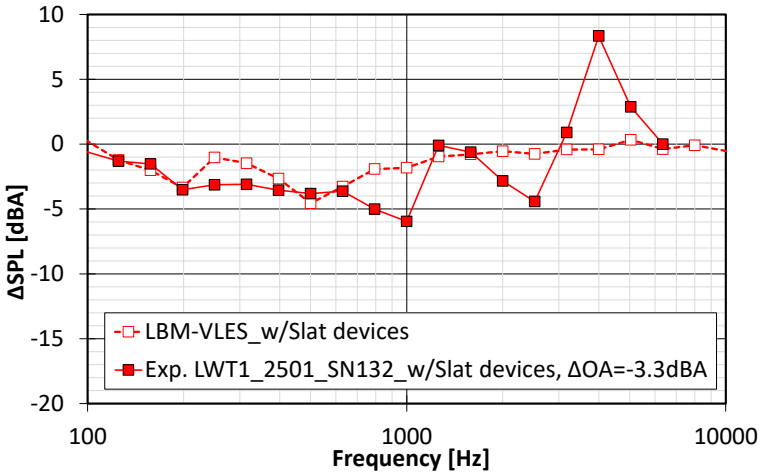
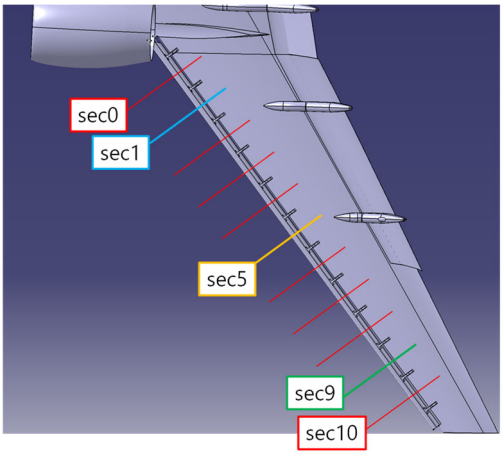
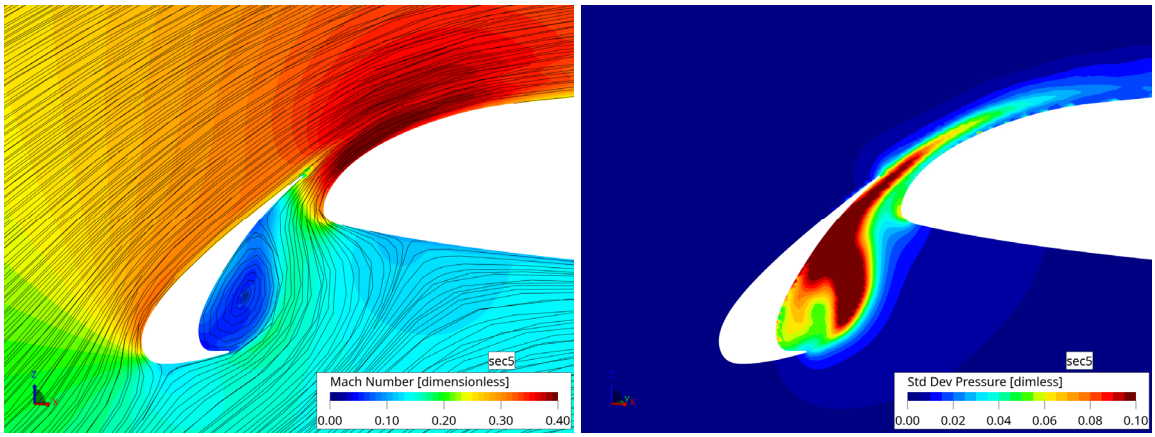


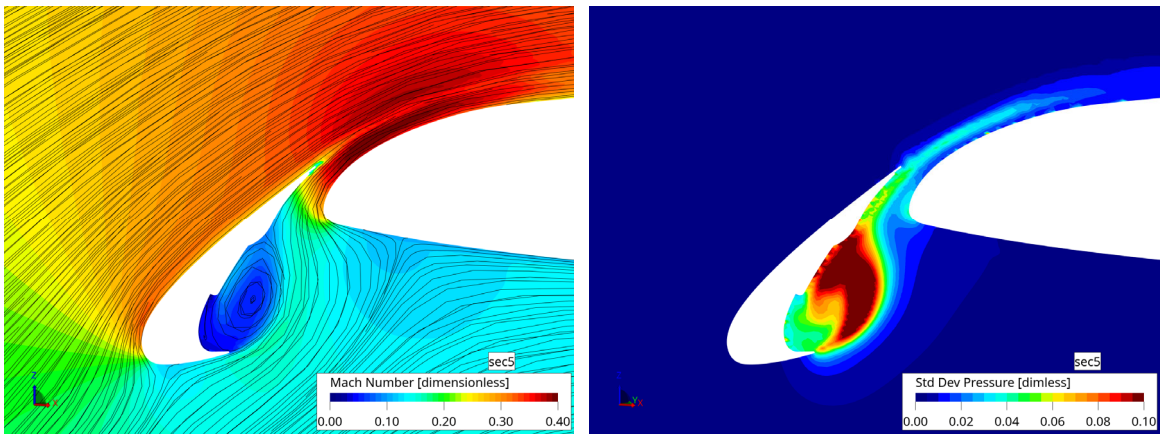
Figure 15 - Comparison of ΔSPL by the slat noise reduction devices, relative to the baseline configuration around the outboard slat at a directivity angle of 98 degrees between computational and wind tunnel test results (converted to full scale).





(i) Mach number and streamlines (ii) wall pressure fluctuation

(a) Baseline configuration without slat noise reduction device



(i) Mach number and streamlines (ii) wall pressure fluctuation

(b) Configuration with slat noise reduction device

Figure 16 – Comparison of sectional views of computational results at Section 5, passing through the mid-span of the outboard slat, for the configurations with and without slat noise reduction devices.

6. Summary

This paper has presented an overview of JAXA's aeroacoustic research in the FQUROH-2 project, which aims to demonstrate the effectiveness of low-noise concepts applied to a generic aircraft model, the CRM-HL, and to validate CFD-based prediction methods. Selected representative results obtained so far have been highlighted, based on acoustic measurements from the first wind tunnel test conducted between April and May 2025 in LWT1 and the corresponding CFD simulations.

The results clearly demonstrate the effectiveness of the slat noise-reduction devices. Compared with

the baseline configuration, the configuration with the slat devices significantly reduces noise across nearly all frequency bands below 3 kHz. A significant overall noise reduction exceeding 3dBA is obtained for the outboard slat.

Comparison studies between the computational and experimental results for the CRM-HL demonstrate the reasonable accuracy of current CFD-based prediction methods for slat noise in the baseline configuration, as well as for predicting ΔSPL by noise reduction devices for realistic high-lift configurations. The computational results also provide physical insights into the noise generation and reduction mechanisms associated with slat cove flows and their change by the slat noise reduction devices.

The ongoing series of wind tunnel tests and CFD activities will further expand the experimental database and continue validation efforts, contributing to the development of reliable prediction methodologies and the practical implementation of airframe noise reduction technologies.

7. Acknowledgments

The authors would like to acknowledge K. Tanaka and T. Hirai of Ryoyu Systems Co. Ltd., and K. Shimoda of IHI Aerospace Engineering Ltd. for their contributions to the preparation and execution of the wind tunnel tests, as well as S. Hagiwara and T. Homma of IHI Aerospace Engineering Ltd. for their contributions to data acquisition. The authors would like to acknowledge T. Hirai and K. Tanaka of Ryoyu Systems Co. Ltd. for their contributions to the preparation and execution of the CFD/CAA computations.

8. Contact Author Email Address

mailto: murayama.mitsuhiro@jaxa.jp

9. Copyright Statement

The authors confirm that they, and/or their company or organization, hold copyright on all of the original material included in this paper. The authors also confirm that they have obtained permission, from the copyright holder of any third party material included in this paper, to publish it as part of their paper. The authors confirm that they give permission, or have obtained permission from the copyright holder of this paper, for the publication and distribution of this paper as part of the ICAS proceedings or as individual off-prints from the proceedings.

References

[1] Yamamoto, K., Hayama, K., Kumada, T., and Hayashi, K., “FQUROH: A Flight Demonstration Project for Airframe Noise Reduction Technology,” *CEAS Aeronautical Journal*, Vol.10, No.1, 2019, pp.77-92.

[2] Yamamoto, K., Takaishi, T., Murayama, M., Yokokawa, Y., Ito, Y., Kohzai, M., Arizono, H., Sakai, R., Shoji, H., Ueno, Y.,Tsuchimoto, Y., Isotani, K., Hayama, K., Kumada, T. and Shimada, A., “FQUROH: A Flight Demonstration Project for Airframe Noise Reduction Technology – the 2nd Flight Demonstration,” AIAA Paper 2018-4087, 2018.

[3] Murayama, M., Takaishi, T., Ito, Y., Yokokawa, Y., Yamamoto, K., Sakai, R., Hirai, T., and Tanaka, K., “Numerical Simulation of Main Landing Gear Noise Reduction in FQUROH Flight Demonstration,” AIAA Paper 2019-1836, 2019.

[4] Murayama, M., Yokokawa, Y., Ito, Y., Takaishi, T., Yamamoto, K., Sakai, R., Hirai, T., and Tanaka, K., “Computational Analysis of Noise Reduction Results for Flap Side-edges in the FQUROH Flight Demonstration Project,” AIAA Paper 2019-2577, 2019.

[5] Ito, Y., Takaishi, T., Shoji, H., Shimada, A., Hayashi, K., and Ueno, Y., “Further Noise Reduction of Regional Jet Two-Wheel Main Landing Gear,” *Journal of Aircraft*, Vol. 62, No. 5, September 2025, pp. 1346-1362.

[6] Murayama, M., Yamamoto, K., Ito, Y., Takaishi, T., Yokokawa, Y., Hirai, T., and Tanaka, K., “Study on Side-edge Geometry of Porous-Plate for Reduction of Airframe Noise from Landing Gear,” AIAA Paper 2023-4174, 2023.

[7] Yamamoto, K., Murayama, M., Isotani, K., Ueno, Y., Hayashi, K., and Hirai, T., “Slat Noise Reduction Based on Turbulence Attenuation Downstream of Shear-layer Reattachment,” AIAA Paper 2022-2954, 32nd AIAA/CEAS Aeroacoustics Conference, June 2022.

[8] Murayama, M., Sakai, R., Ito, Y., Kohzai, M., Yokokawa, Y., Ura, H., Yamamoto, K., Takaishi, T., Hayashi, K., Ueno, Y., et al., “Noise Reduction Design for High Lift Devices of Regional Jet,” 28th AIAA/ CEAS Aeroacoustics Conference, AIAA Paper 2022-2955, June 2022.

[9] JAXA Press Release, “Establishment of Joint Research Structures for Airframe Noise Reduction of Medium Size Passenger Aircraft,” August 2021, https://global.jaxa.jp/press/2021/08/20210820-1_e.html (cited 01 June 2026).

[10] Lacy, D. S., and Sclafani, A. J., “Development of the High Lift Common Research Model (HL-CRM): A Representative High Lift Configuration for Transonic Transports”, AIAA Paper 2016-0308, 54th AIAA Aerospace Sciences Meeting, January 2016.

[11] Lacy, D. S. and Clark, A. M., “Definition of Initial Landing and Takeoff Reference Configurations for the High Lift Common Research Model (CRM-HL)”, AIAA-2020-2771, AIAA Aviation Forum, June 2020.

[12] Hashioka, T., Murahashi, Y., Yasuda, H., Sawaki, Y., Onda, S., Tsuchimoto, Y., Nishizaki, Y., Suzuki, W., and Kawamura, T., “Test Summary of the Full-Span High-Lift Common Research Model at KHI aero-acoustic Low-Speed Wind Tunnel,” 34th Congress of the International Council of the Aeronautical Sciences, 2024.

[13] Evans, A., Lacy, D., Smith, I. and Rivers, M., “Test Summary of the NASA Semi-Span High-Lift Common Research Model at the QinetiQ 5-Metre Low-Speed Wind Tunnel,” AIAA Paper 2020-2770, June 2020. doi:10.2514/6.2020-2770.

[14] Lockard, D. P., Turner, T. L., Bahr, C. J., and Hutcheson, F. V., “Overview of Aeroacoustic Testing of the High-Lift Common Research Model,” AIAA2021-2113, AIAA Aviation Forum, 2021.

[15] Ertsgaard, M. L., and Winski, C. S., “Development of NASA 5.2% Semispan High Lift Common Research Model (CRM-HL),” AIAA2025-1127, 2025.

[16] Pülm, S., Schmidt, F. N., Rudnik, R., and Winski, C. “Low-Speed Testing of the 5.2% Semispan CRM-HL in the DNW-NWB Wind Tunnel”, AIAA paper 2024-3516, AIAA Aviation Forum and Ascend 2024, July 2024.

[17] Mouton, S., Charpentier, G., and Lorenski, A., “Test Summary of the Full-Span High-Lift Common Research Model at the ONERA F1 Pressurized Low-Speed Wind Tunnel,” AIAA Paper 2023-0823, January 2023.

[18] Mouton, S., and Davy, R., “Aeroacoustic Testing of the High-Lift Common Research Model at the ONERA F1 Pressurized Low-Speed Wind Tunnel,” AIAA Paper 2024-3513, July 2024.

[19] Kohzai, M., Murayama, M., Murata, Y., Ura, H., Ito, Y., and Takaishi, T., “JAXA’s Test Plans and Preliminary Low-speed Wind Tunnel Test Results with 8% Scale Semispan High Lift Common Research Model,” 2025 AIAA AVIATION Forum, Las Vegas, NV, July 2025 (presentation only).

[20] Murata, Y., Murayama, M., Kohzai, M., Yamamoto, K., Ura, H., Ito, Y., and Takaishi, T., “Aeroacoustic Testing of JAXA 8% Semispan High-Lift Common Research Model (CRM-HL) with Low-Noise Concepts,”

AIAA Paper 2026-3427, May 2026.

[21]Murata, Y., Murayama, M., Kohzai, M., Yamamoto, K., Ura, H., Ito, Y., Takaishi, T., Choudhari, M. M., and Lockard, D. P., “Model-Configuration Effects in Aeroacoustic Testing of the JAXA 8% CRM-HL,” AIAA Paper 2026-3428, May 2026.

[22]Ito, Y., Takaishi, T., Ozawa, Y., and Hirai, T., “Aeroacoustic Characteristics of Main Landing Gear of High-Lift Common Research Model,” AIAA Paper 2025-3282, July 2025.

[23]Ito, Y., Takaishi, T., Ozawa, Y., Kohzai, M., and Jawahar, H. K., “Main Landing Gear Noise Reduction Impact on JAXA 8% Semispan High-Lift Common Research Model,” AIAA Paper 2026-3479, May 2026.

[24]Ozawa, Y., Ito, Y., Takaishi, T., Shimoda, K., Hirai, T., and Jawahar, H. K., “Effect of Noise-reduction Devices on Wake Flow Behind Main Landing Gear of High-Lift Common Research Model,” AIAA Paper 2026-3480, May 2026.

[25]Suzuki, T., Murayama, M., Yamamoto, K., and Hirai, T., “Noise Prediction of NASA CRM-HL Using Lattice-Boltzmann Method and Wall-Modeled LES,” AIAA Paper 2025-3277, July 2025.

[26]Murayama, M., Yamamoto, K., Murata, Y., Kohzai, M., Hirai, T., and Suzuki, T., “CRM-HL Noise Prediction Based on LBM-VLES Compared with a Wind-tunnel Test,” AIAA Paper 2026-3426, May 2026.

[27]Asada, H., Maeyama, H., Kawai, S., Murayama, M., Kohzai, M., Murata, Y., Yamamoto, K., and Kawai, S., “Wall-Modeled LES of Aeroacoustic Flows Around NASA CRM-HL Using Fully Automated Cartesian-Grid-Based Solver FFVHC-ACE,” AIAA Paper 2026-3258, May 2026.

[28]Kohzai, M., Murayama, M., Sansica, A., Takaishi, T., and Abe, H., “Aerodynamic characteristics of 8% Scale Semispan High Lift Common Research Model at the JAXA 6.5m x 5.5m Low Speed Wind Tunnel,” ICAS 2026 (to be presented).